BIOCHEMISTRY
including biophysical chemistry & molecular biology

Article

pubs.acs.org/biochemistry

Molecular Modeling of the Reaction Pathway and Hydride Transfer Reactions of HMG-CoA Reductase

Brandon E. Haines,[†] C. Nicklaus Steussy,[‡] Cynthia V. Stauffacher,[‡] and Olaf Wiest*[,†]

[†]Department of Chemistry and Biochemistry, Notre Dame University, Notre Dame, Indiana 46556, United States

[‡]Department of Biological Sciences, Purdue University, West Lafayette, Indiana 47907, United States

Supporting Information

ABSTRACT: HMG-CoA reductase catalyzes the four-electron reduction of HMG-CoA to mevalonate and is an enzyme of considerable biomedical relevance because of the impact of its statin inhibitors on public health. Although the reaction has been studied extensively using X-ray crystallography, there are surprisingly no computational studies that test the mechanistic hypotheses suggested for this complex reaction. Theozyme and quantum mechanical (QM)/molecular mechanical (MM) calculations up to the B3LYP/6-31g(d,p)//B3LYP/6-311++g(2d,2p) level of theory were employed to generate an atomistic description of the enzymatic reaction process and its energy profile. The models generated here predict that the catalytically important Glu83 is protonated prior to hydride transfer and that it acts as the general acid or base in the reaction. With Glu83 protonated, the activation energies calculated for the sequential hydride transfer reactions, 21.8 and 19.3 kcal/mol, are in qualitative agreement with the experimentally determined rate constant for the entire reaction (1 s^{-1} to 1 min^{-1}). When Glu83 is not protonated, the first hydride transfer reaction is predicted to be disfavored by >20 kcal/mol, and the activation energy is predicted to be higher by >10 kcal/mol. While not involved in the reaction as an acid or base, Lys267 is critical for stabilization of the transition state in forming an oxyanion hole with the protonated Glu83. Molecular dynamics simulations and MM/Poisson−Boltzmann surface area free energy calculations predict that the enzyme active site stabilizes the hemithioacetal intermediate better than the aldehyde intermediate. This suggests a mechanism in which cofactor exchange occurs before the breakdown of the hemithioacetal. Slowing the conversion to aldehyde would provide the enzyme with a mechanism to protect it from solvent and explain why the free aldehyde is not observed experimentally. Our results support the hypothesis that the pK_a of an active site acidic group is modulated by the redox state of the cofactor. The oxidized cofactor and deprotonated Glu83 are closer in space after hydride transfer, indicating that indeed the cofactor may influence the pK_a of Glu83 through an electrostatic interaction. The enzyme is able to catalyze the transfer of a hydride to the structurally and electronically distinct substrates by maintaining the general shape of the active site and adjusting the electrostatic environment through acid−base chemistry. Our results are in good agreement with the well-studied hydride transfer reactions catalyzed by liver alcohol dehydrogenase in calculated energy profile and reaction geometries despite different mechanistic functionalities.

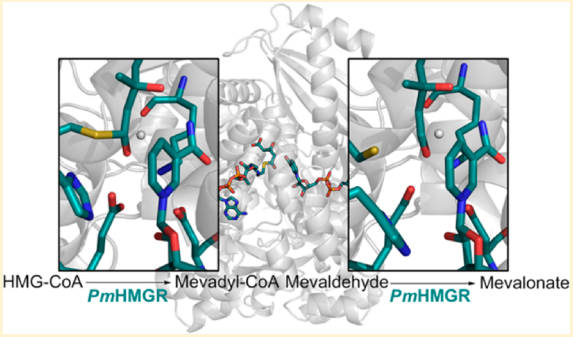

HMG-CoA reductase (HMGR) is an NAD(P)H-dependent four-electron oxidoreductase that catalyzes the interconversion of HMG-CoA and mevalonate as shown in Scheme 1. This reaction is the point of feedback control for the mevalonate pathway, which is responsible for the biosynthesis of many important isoprenoid compounds, including precursors to cholesterol in humans.[1] HMGR is the target of a class of drugs called statins that are used to treat hypercholesterolemia and reduce the risk of cardiovascular disease. Because of the extensive use of these drugs and the large public health impact they have in developed countries, most of the attention garnered by HMGR is focused on the pharmacology of statin use and general inhibition of the enzyme.[2] Other active research fields include the drug design of statin alternatives for the human HMGR (class I) and antimicrobial agents to target

Scheme 1. Reactions Catalyzed by HMG-CoA Reductase

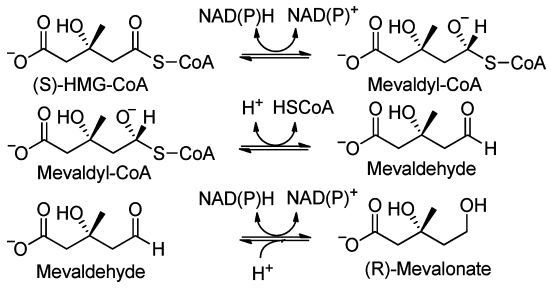

Received: June 27, 2012
Revised: September 11, 2012
Published: September 12, 2012

dx.doi.org/10.1021/bi3008593 | *Biochemistry* 2012, 51, 7983−7995

the evolutionarily divergent HMGRs of pathogenic bacteria (class II).[3−7]

In comparison, much less work has been devoted to the mechanistic and structural aspects of HMGR.[8] This is surprising given its unique and complex reaction mechanism as well as the fact that it is arguably the most biomedically important enzyme described so far. Crystal structures of human HMGR (hHMGR) and class II HMGR from a soil bacterium (*Pseudomonas mevalonii*, *Pm*HMGR) have provided a foundation from which to build a more detailed reaction mechanism.[9−12] Multiple studies have been performed for *Pm*HMGR that have established its precedent as a model HMGR in the literature,[13] granted minor structural and functional differences between classes, e.g., cofactor specificity[14−16] and stereochemistry of the hydride transfer.[10,11,17,18] This model HMGR has a large number of crystal structures available and several interesting features in that the reaction can be run in either direction and the protein crystals are stable to a variety of conditions. However, results from X-ray crystallography inherently contain only indirect information about the chemical steps and cannot observe key reaction species such as transition states and, in many cases, intermediates. Most hydrogen atoms, such as those involved in the reduction steps of HMGR, are not observed directly, and therefore, the protonation states of ionizable residues are commonly speculative. In addition, these structural models do not provide energetic information, which limits the ability of the researcher to test mechanistic hypotheses.

The *Pm*HMGR forward reaction selectively produces one molecule of the product alcohol, (*R*)-mevalonate, from the substrate, (*S*)-HMG-CoA, for every two molecules of oxidized cofactor.[19,20] This creates a unique reaction sequence because the successive, stereospecific two-electron reduction steps take place in a single active site. As shown in Scheme 1, the reaction is thought to proceed through two intermediates, a hemithioacetal and an aldehyde. Initially, the hemithioacetal was hypothesized to be a reaction intermediate because preformed mevaldyl-CoA is quickly reduced by the enzyme.[19] A hemithioacetal structural analogue produced from a slow substrate, dithio-HMG-CoA, was recently found in the active site of a *Pm*HMGR crystal structure alongside an oxidized cofactor molecule.[21] This structure is important because the enzyme is active in the crystal, which makes observation of the full array of natural intermediates difficult. Despite a slightly larger tetrahedral shape, the hemidithioacetal mimics the hemithioacetal intermediate in functional group position and presumably specific interactions with the enzyme. The crystal structure is an indication that the enzyme active site is suitable for favorable binding of a tetrahedrally shaped species, providing further justification of the likelihood of a persistent hemithioacetal intermediate.

Mevaldehyde is often considered to be an intermediate on the basis of its electrophilic nature and because it can be used as an enzymatic substrate in either oxidation to mevalonate or reduction to HMG-CoA.[22] However, free mevaldehyde is not detected during the reaction in experiments using isotope dilution or semicarbazide trapping.[23,24] Additionally, if the reaction is run in a pool of radioisotopic mevaldehyde, no heavy atoms are incorporated into the mevalonate product despite binding constants in the micromolar to millimolar range and solvent exposure of the active site during the reaction.[22,25,26] It is therefore clear that if mevaldehyde is a reaction intermediate, it does not dissociate from the active site. There is also no crystallographic evidence of the aldehyde intermediate as neither mevaldehyde nor any structural analogue has been trapped yet in a crystal structure of *Pm*HMGR.[27] These results have led to hypotheses that the hemithioacetal is the reaction intermediate and that perhaps the steps following the formation of mevaldehyde are fast enough that it does not accumulate in any appreciable amount.[19,23,24]

Early pH dependence studies of the reaction identified a protonated histidine and aspartate/glutamate pair in the active site.[28] Site-directed mutagenesis experiments confirmed the essentiality of these residues, along with an additional aspartate residue in multiple HMGRs.[29−32] The histidine was assigned the role of proton donor for the CoA thiolate anion after hemithioacetal breakdown.[31,32] The first crystal structure of *Pm*HMGR revealed that the enzyme forms a homodimer with the active site located at the interface of the monomers.[12,33] The conserved residues, Glu83 and Asp283, are positioned in the active site around a lysine residue, Lys267.[12] The lysine is highly conserved and was subsequently found to be essential to enzyme activity through site-directed mutagenesis experiments.[11] Recently, a series of crystal structures discovered specific interactions among CoA, His381, and a conserved serine residue, Ser85, to form a hydrogen bonding network important for positioning of His381 and the thioester of HMG-CoA.[21] While Ser85 is not thought to be chemically involved in the hydride transfer reactions, site-directed mutagenesis experiments show enzyme activity is drastically reduced when it is mutated to an alanine.[21]

The original crystal structure showed that the 50 C-terminal residues, including the catalytic histidine (His381), were unresolved in the electron density. This domain was named the flap domain, and the authors speculated that it could close to position the histidine correctly in the active site and protect the hydride transfer reactions from solvent.[12] Later, the crystal structure of the nonproductive *Pm*HMGR−HMG-CoA−NAD^+ ternary complex was determined as shown in Figure 1. This structure provides insight into how the substrate and cofactor fit into the active site and implies a connection between ligand binding and the state of the flap domain. HMG-CoA binds in the large domain, while the cofactor binds to a nonclassical

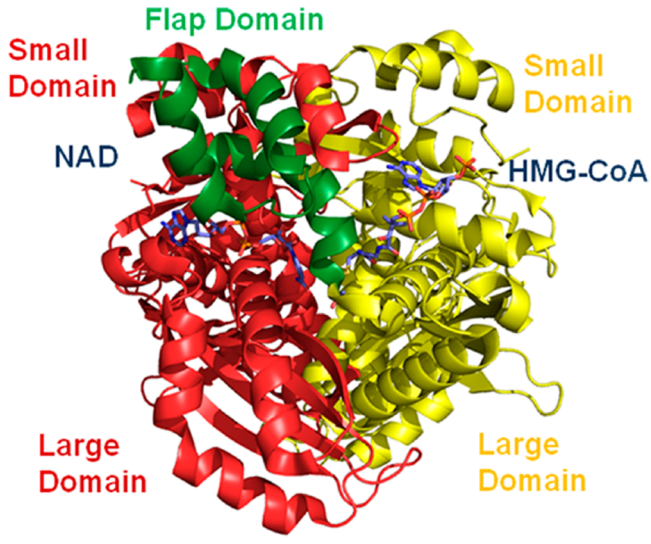

Figure 1. Crystal structure of the *Pm*HMGR−HMG-CoA−NAD^+ ternary complex (Protein Data Bank entry 1QAX).[11]

dx.doi.org/10.1021/bi3008593 | *Biochemistry* 2012, 51, 7983−7995

dinucleotide-binding fold in the small domain. Additionally, this structure contained electron density for the flap domain (colored green in Figure 1), which is closed over the active site in a three-helix bundle making specific interactions with the cofactor.[11] The catalytic histidine is located on the innermost helix of the flap domain and is positioned near HMG-CoA. This finding poses the intriguing question of the role of the opening and closing of the flap domain for the overall reaction mechanism. Taking into consideration this process, the cofactor exchange step, the two distinct chemical reactions shown in Scheme 1, and the nature of the reaction intermediates, it is clear that the overall reaction sequence is very complex and the current models for the reaction are insufficient to completely describe it. A minimal model of the reaction mechanism would thus have to include flap domain opening and closing sometime after the first reduction step, a tightly controlled conversion between the previously described intermediate states, and some sort of coupling between them.

There are also several open questions about the mechanisms of the chemical steps of the reaction. The details of the proposed double-hydride transfer mechanisms and the assignment of the roles of the catalytic residues remain ambiguous. The cationic His381 is thought to be responsible for protonation of the expelled CoA thiolate anion after the first hydride transfer step. The anionic Asp283 is proposed to support the position of an essential positive charge in the oxyanion hole, which is provided by the cationic Lys267.[11,34] However, the roles of Glu83 and Lys267 are not clear from the available crystal structures. It appears that the most likely mechanism is linked to the most likely protonation state of Glu83 in the *Pm*HMGR active site environment. An unprotonated Glu83 would support Lys267 in the oxyanion hole as a secondary hydrogen bond acceptor. As shown in Scheme 2a, this would designate Lys267 as the general acid

Scheme 2. Possible Mechanisms for *Pm*HMGR Based on the Protonation State of Glu83[a]

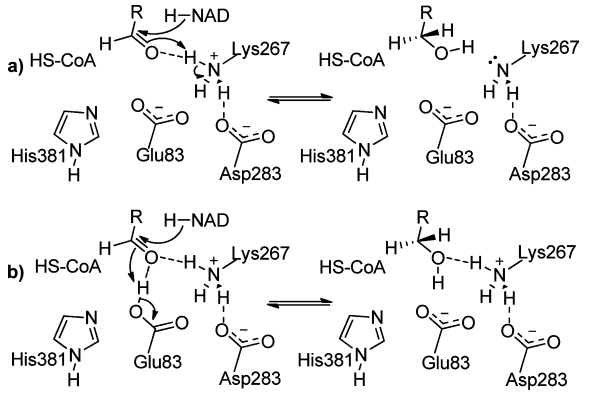

[a](a) Glu83 is not protonated prior to hydride transfer, and Lys267 acts as the proton donor to mevalonate. (b) Glu83 is protonated prior to hydride transfer and acts as the proton donor to mevalonate.

responsible for protonation of the product mevalonate after the second hydride transfer.[11] However, it has been suggested from the hHMGR structure that the proximity of the negatively charged residues, Glu83 and Asp283, would increase the pK_a of the glutamate residue so that it is protonated prior to hydride transfer.[10] If Glu83 is protonated, it is close enough to be the second component of the oxyanion hole and would presumably act as the general acid in the final protonation step as depicted in Scheme 2b. On the basis of the available crystal structures, it is possible that either or both mechanisms are relevant.

A fascinating aspect of the catalysis of HMGR is the ability to reduce two sterically and electronically different substrates in the same active site and to run the reaction for mevaldehyde in either direction. Considering the widespread interest in the mechanism of enzymatic hydride transfer,[35−38] it is surprising that these aspects of the HMGR mechanism have not received much attention in the past and that, to the best of our knowledge, no computational studies of HMGR have been published thus far. A similar NAD-dependent enzyme that acts through a hydride transfer mechanism is liver alcohol dehydrogenase (LADH), whose mechanism has been studied in much greater detail than that of HMGR. Specifically, the ability of LADH to either reduce or oxidize aldehydes has been investigated computationally.[39−42] The transition structure for LADH aldehyde oxidation is a suitable comparison for the HMGR thioester reduction step, while the transition structure for LADH alcohol oxidation is a suitable comparison to the HMGR aldehyde reduction step. These comparisons can offer insight into the mechanism by which dual-hydride transfer enzymes can efficiently catalyze hydride transfer to dissimilar substrates and can also be applied to other thioester reducing enzymes.

This study uses a combination of classical mechanics (MM), quantum mechanics (QM), and hybrid methods to address the open questions regarding the mechanism of HMGR. (i) Why is the putative aldehyde intermediate not observed experimentally? (ii) What are the mechanisms of the separate hydride transfer reactions, and how do they compare to each other as well as to related hydride transfer reactions? (iii) What are the roles of the active site residues in catalyzing two distinct hydride transfer reactions in the same active site? (iv) What is the protonation state of the crucial Glu83, and what is its role in the hydride transfer reaction mechanisms?

METHODS

Molecular Dynamics Simulations. The structures relevant for the reaction are the HMG-CoA−NADH (ES), mevaldyl-CoA−NAD^+ (EI1P), mevaldyl-CoA−NADH (EI1H), mevaldehyde−NADH (EI2), and mevalonate−NAD^+ (EP) complexes. They were built from either the nonproductive HMG-CoA−NAD^+ complex [Protein Data Bank (PDB) entry 1QAX] or the hemidithioacetal−NAD^+ complex.[11,21] Published force field parameters and charges were used for the NADH and NAD^+ molecules.[43,44] All other ligands were optimized using AM1 in the G09 suite of programs,[45] and atom-centered partial charges were generated using HF/6-31g* and the AMBER antechamber program with RESP fitting.[46−48] The protonation states of the individual residues were assigned using the Poisson−Boltzmann method via the H++ program at pH 7, followed by manual inspection.[49,50] The active site histidine (H381) implicated in catalysis was modeled as positively charged,[11,28,32] and both protonation states were studied for Glu83. Models were solvated in a periodic box of TIP3P[51] waters extending 10 Å from each solute atom. The net charge was neutralized with Na^+ ions depending on the protonation state of Glu83 by LEaP. The ff03.r1 all atom AMBER force field[52] was employed in addition to GAFF for the simulations.[53]

Simulations were performed with either PMEMD or SANDER within the AMBER 11.0 suite of programs.[45] A 2 fs time step was chosen, and the SHAKE algorithm[54] was used

dx.doi.org/10.1021/bi3008593 | *Biochemistry* 2012, 51, 7983−7995

to constrain all bonds containing hydrogen. The nonbonded cutoff was set to 10.0 Å, and the nonbonded pair list is updated every 25 steps. The pressure (1 atm) and temperature (300 K) were controlled with a Berendsen's barostat and thermostat, respectively.[55,56] Periodic boundary conditions were applied to simulate a continuous system, and the particle mesh Ewald (PME) method was employed to include the contributions of long-range interactions.[57,58] A position-constrained minimization was performed to relax the water molecules followed by a full minimization to relax any close contacts. All simulations were run for at least 20 ns with an equilibration period of 800 ps. For some of the complexes, weak harmonic restraints were applied to certain distances for up to 200 ps during equilibration. Coordinates were saved every 10 ps, and trajectories were analyzed using the PTRAJ program of AMBER.

Molecular Mechanics (MM)/Poisson−Boltzmann Surface Area (PBSA) Rescoring. The MMPBSA.py program in AmberTools 1.5 was used to calculate the binding free energy, ΔG_{bind}.[45] ΔG_{bind} is estimated from "gas phase" ligand−protein interactions, ΔG_{MM}, and solvation contributions, ΔG_{solv}. The conformational entropy was ignored in the interest of computational expense. Snapshots were taken at 10 ps intervals from the MD simulation trajectories totaling between 700 and 800 frames for each complex. A limitation for comparing the relative ΔG_{bind} of the relevant *Pm*HMGR complexes is the fact that the charge states of the receptor and cofactor change. To corroborate the ΔG_{bind} values, three cases were calculated for each complex: both cofactor and substrate defined as the ligand against the protein as the receptor, only the substrate defined as the ligand against the cofactor and protein as the receptor, and only the cofactor defined as the ligand against the substrate and protein as the receptor. The ΔG_{bind} values of these cases can be subtracted to isolate the ΔG_{bind} values of individual substrates and cofactors to eliminate the errors associated with comparing complexes with different charge states. We can then cross-reference the ΔG_{bind} values of both ligands and therefore whole complexes with the ΔG_{bind} of the individual substrates and cofactors to validate them. The value of the exterior dielectric constant is set to 80, and the internal dielectric constant is set to 1. It should be noted that MM/PBSA rescoring is a fast but limited free energy approach, and only qualitative trends are inferred from these results. More rigorous free energy calculations or further experiments would be necessary to gain a more quantitative description of the relative energies between the complexes along the reaction coordinate. However, this is beyond the scope of this mechanistic study.

Quantum Mechanical Models. The theoretical enzyme (theozyme) is a predicted catalytic array of biologically occurring functionalities acting to stabilize the transition state of a given biochemical reaction.[59,60] Theozymes are small enough to be treated wholly with high-level QM methods, but the minimal model lacks the protein environment that the reaction experiences naturally. For example, secondary hydrogen bonds and protein secondary structure elements are replaced with unphysical atom-centered constraints to hold a residue near its crystallographic position. In contrast, hybrid quantum mechanics/molecular mechanics (QM/MM) calculations allow for the entire protein environment to be included in the reaction description but are more computationally demanding and do not treat the system at a consistent level of theory.[61] They thus require careful treatment of the boundary region where the models are to be treated at two different levels of theory. Theozyme and QM/MM models are complementary to each other because of a trade-off between accuracy and computational expense. For this study, a typical work flow begins with a theozyme model extracted from the coordinates of an MD simulation. Parameters from the theozyme model are then used to build a whole protein model for QM/MM calculations. Comparison of the energies between models can also be useful for cases where known errors are identified.

The theozyme models contain residue fragments of Glu83 (CH_3CO_2H or $CH_3CO_2^-$), Asp283 ($CH_3CO_2^-$), Lys267 ($CH_3CH_2NH_3^+$), and His381 ($CH_3C_3H_5N_2^+$ or $CH_3C_3H_4N_2$) with the terminal methyl group frozen. The NAD cofactor was modeled using a nicotinamide ring capped with a methyl group; the substrate was cleaved between the carbon−carbon bond before the first peptide bond, and the carboxy group of the substrate was excluded. A sample theozyme structure is shown in Figure S1 of the Supporting Information. Ser85 was not included in the QM calculations because it does not appear to affect the position of the reactants on the time scales examined, i.e., directly before or after hydride transfer. However, it is noted that a full description of the reaction must include a more refined role for Ser85. The QM calculations were conducted with the G09 suite of programs at the B3LYP/6-31g(d,p)//B3LYP/6-311++g(2d,2p) level of theory.[45] The integral equation formalism implementation of the polarizable continuum model[62−64] (IEFPCM) was applied with $\varepsilon = 6$ to mimic the internal dielectric constant of a protein environment.[65] Constrained geometry optimizations were performed for intermediates or transition states. Frequency calculations were used to characterize the structures either as a ground state (zero negative frequencies) or as a transition state (exactly one negative frequency). Residual, low negative frequencies are common in such calculations because of the constraints being placed on the system. These frequencies are visually inspected to ensure that they are localized near the constrained atoms or that they do not resemble bond breaking or forming processes. All energies are Gibbs free energies calculated at 298 K and 1 atm of pressure. It should be emphasized again that these are only estimates of the Gibbs free energies because of the constraints used. However, it was shown previously that the estimates provided by this approach are in good agreement with both experimental values and other computational studies.[66] All distances are reported in angstroms, and angles are reported in degrees. Hydrogen bond distances are reported from heavy atom to heavy atom unless otherwise noted.

The two-layer ONIOM method as implemented in the G09 suite of programs was used for QM/MM calculations.[67,68] The initial guesses for the reactant structures of the first and second hydride transfer reaction were built from snapshots of the HMG-CoA−NADH and mevaldehyde−NADH trajectories, respectively. These structures were first subjected to geometry optimization with AMBER 11.0 to gain a good initial geometry. The layers were partitioned as shown in Figure 2 with the link atoms highlighted in magenta. The QM regions of the first and second hydride transfer reaction consist of 105 and 96 atoms, respectively, and six hydrogen link atoms. Because the active site is shielded from solvent by the flap domain, all water molecules were deleted. All counterions were maintained to keep the system neutral, and all atoms outside a 7 Å radius around the QM atoms were frozen.

Geometry optimizations were performed using the ONIOM-(B3LYP/6-31g(d,p):AMBER) method. The ONIOM mechanical embedding (ME) scheme was used for geometry

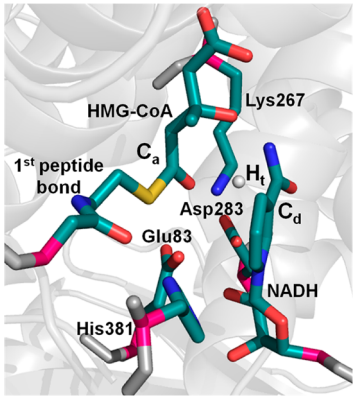

Figure 2. ONIOM partitioning scheme. The QM region is colored by element; link atoms are colored magenta, and the MM region is colored gray. Hydrogen atoms were omitted for the sake of clarity.

optimization, and the ONIOM electronic embedding (EE) scheme was used for single-point calculations at the ONIOM-(B3LYP/6-31g(d,p):AMBER) and ONIOM(B3LYP/6-311++g(2d,2p):AMBER) levels. Because of significant differences in the active site electrostatics between the enzyme complexes along the reaction pathway, the iterative method for updating the partial charges in the MM charges of the atoms in the QM region developed by Tao et al. was used.[69] The entire system (>12000 atoms) is too large for a full frequency calculation. Thus, only the 15 lowest modes were calculated using the freq=(Nfreq=N) keyword in G09 to characterize the ground states and transition states. The reactants and products have no negative frequencies, and the transition states have exactly one negative frequency.

RESULTS

Michaelis Complex. The model formulated from docking calculations by Steussy et al. describes the initial stages of the reaction.[21] For the purposes of this study, the calculated energy profile begins at the HMG-CoA binary complex (PDB entry 1R31) and proceeds to the hemidithioacetal−NAD^+ ternary complex through a "transition state" modeled by the non-productive HMG-CoA−NAD^+ ternary complex (PDB entry 1QAX), where the thioester moiety of HMG-CoA is pointed toward Glu83 and Lys267. This transition state model mimics the Michaelis complex. We hypothesized that the non-productive HMG-CoA−NAD^+ complex is a reasonable model for the Michealis complex and could serve as an initial guess of the conformation of the enzyme immediately before hydride transfer. The complex should be a minimum on the potential energy surface and should be easily probed via classical MD simulations but resemble a prereaction complex. Indeed, in an MD simulation, the HMG-CoA−NADH ternary complex built from PDB entry 1QAX is stable over 20 ns. The interactions between the thioester oxygen and Glu83 and Lys267 are stable over that time period, and the average hydride acceptor carbon−hydride donor carbon (C_a−C_d) distance is 3.5 Å, as shown in Figure S2a of the Supporting Information. Using the structure of PDB entry 1QAX as a model for the Michaelis complex is therefore justified.

Further comparison of the 1QAX crystal structure with snapshots from the MD simulations, as shown in Figure 3, reveals that the structures are similar in the active site. The positions of the cofactor NAD and important residues are in good agreement. The biggest differences between the structures

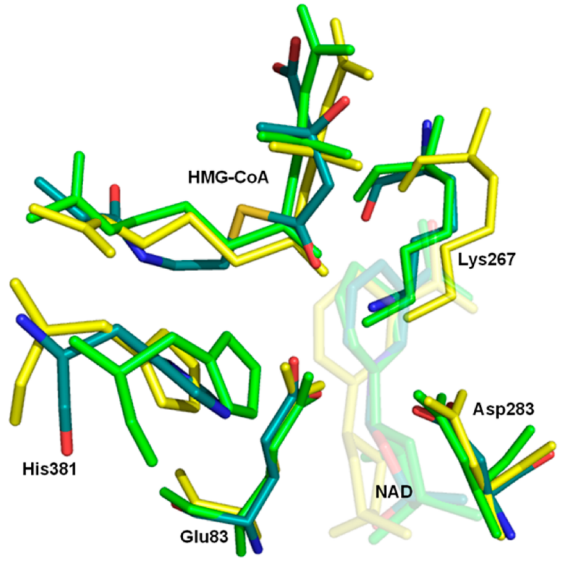

Figure 3. Overlay of the *Pm*HMGR active sites of 1QAX (colored by element), neutral Glu83 (yellow), and anionic Glu83 (green). Hydrogen atoms and the main chain atoms for His381 were omitted for the sake of clarity.

are in the area between the first peptide bond (as defined in Figure 2) and the thioester in the HMG-CoA substrate. In the 1QAX structure (colored by atom in Figure 3), the sulfur atom points away from His381, whereas in the models produced from the MD simulations (colored green and yellow in Figure 3), the sulfur atom points toward His381. These structural differences can be rationalized by considering the different redox forms of the NAD cofactor and the ambiguity of the protonation state of His381 in the 1QAX crystal structure.

Protonation State of Glu83. To investigate the protonation state of Glu83, a key question for any mechanistic proposal for HMGR, we performed MD simulations on the Michealis complex with either a neutral (yellow in Figure 3) or anionic (green in Figure 3) Glu83 residue. When Glu83 is neutral, the C_a−C_d distance is shorter on average by ∼0.4 Å as shown in Figure S2b of the Supporting Information. This would indicate that the hydride transfer is more likely when Glu83 is protonated. When Glu83 is protonated, the thioester carbonyl is positioned to form interactions in an oxyanion hole with both Glu83 and Lys267. His381 forms the aforementioned hydrogen bond to the carbonyl of the first peptide bond in HMG-CoA and is positioned near the sulfur atom. This position of His381 is consistent with its proposed function in the reaction. When Glu83 is not protonated, the active site clearly reorganizes because of the electrostatic repulsion between the negatively charged Glu83 and Asp283 residues. The thioester carbonyl is pointed toward Lys267, and the active site is distorted relative to the experimentally observed structure. His381 engages in a salt bridge with Glu83, which positions it deeper in the active site and away from the first peptide bond and sulfur of HMG-CoA, in contrast to the X-ray structure. In this position, His381 partially blocks the nicotinamide ring of the cofactor from the thioester, resulting in a longer C_a−C_d distance. Together, these results strongly suggest that Glu83 is protonated in the active form of HMGR.

Next, QM theozyme models for each protonation state were constructed from snapshots from the MD simulations to model the effects of the active site on the reaction. The theozyme

dx.doi.org/10.1021/bi3008593 | *Biochemistry* 2012, 51, 7983−7995

structures for the deprotonated case displaying important geometrical parameters are shown in Figure 4. In the transition

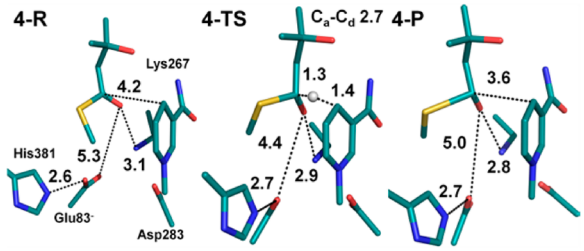

Figure 4. Theozyme models for the reactant, transition state, and product of the first hydride transfer when Glu83 is not protonated.

state model with a protonated Glu83, it and Lys267 form a tight oxyanion hole around the developing oxyanion and the pK_a of Glu83 is sufficiently low to instantaneously donate a proton to stabilize the product species. Conversely, in the transition structure model with Glu83 unprotonated, the oxyanion hole consists of only Lys267, and there is a long distance between Glu83 and the thioester oxyanion. In the product, the proton is not transferred from Lys267 to the thioester oxyanion. Instead, the carbon−sulfur bond lengthens to 2.5 Å, indicating that Lys267 alone is not sufficient to stabilize the experimentally observed hemithioacetal intermediate state.

It is important to note that in the unprotonated Glu83 theozyme model the negatively charged Glu83 is positioned close to the positively charged His381. During the constrained optimization, the proton from His381 is instantaneously transferred to Glu83, and the residues remain hydrogen-bonded. The fact that Glu83 is instantaneously protonated shows that the electrostatic makeup of the active site elevates the pK_a of the Glu83 carboxyl group above that of His381. In other words, the neutrality of Glu83 is necessary to keep the electrostatic environment of the active site such that His381 is protonated. This is consistent with experimental data that suggest His381 must be protonated for NADH to bind and then to conduct its general acid functionality later in the reaction.[28] Second, because the interaction between Glu83 and His381 is maintained, the oxyanion hole still consists of only Lys267.

These results are consistent with the energy profiles shown in Figure 5. The higher activation barrier for the unprotonated versus the protonated model of >10 kcal/mol is likely due to the additional favorable interaction that Glu83 supplies to the oxyanion hole to help Lys267 stabilize the transition state. The intermediate species resulting from the collapse of the hemithioacetal produces a reaction that is endothermic by 20.9 kcal/mol. The pathway producing a protonated hemithioacetal intermediate is exothermic by 0.8 kcal/mol. The difference of >20 kcal/mol in the reaction free energy between the two pathways indicates that the thioester oxyanion must be stabilized by two hydrogen bonds or by a group acidic enough for proton transfer. In the *Pm*HMGR active site, that group cannot be Lys267, and thus, the reaction will be difficult unless Glu83 is protonated and participating in the oxyanion hole. The energies generated from this model represent a lower bound because neutralization of Glu83 through His381 prevents the accumulation of three negatively charged entities (Glu83, Asp283, and the substrate oxyanion) in the same space. Nevertheless, the findings from these simple models support

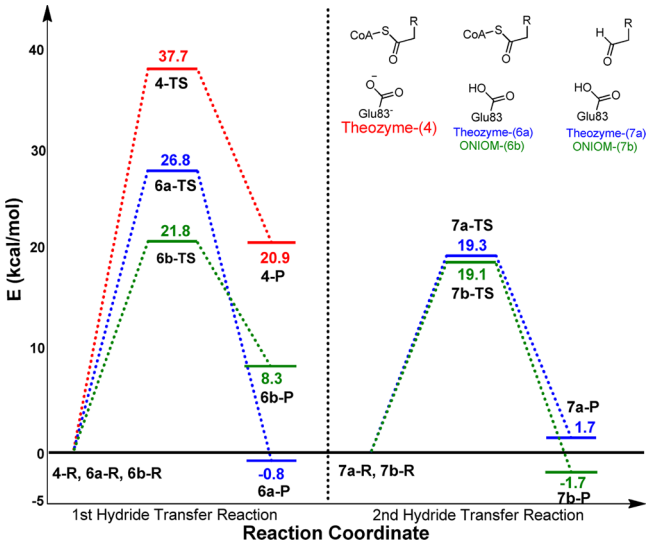

Figure 5. Reaction profiles for *Pm*HMGR with the different methods used. Energies calculated for the theozyme models are colored blue for protonated Glu83 and red for deprotonated Glu83. The ONIOM energies are colored green.

the suggestion that the spatial proximity between the active site glutamate and aspartate residues indicates that one of them is protonated.[10] Protonation of Asp283 is unlikely because of its participation in the structurally important salt bridge with Lys267. Therefore, the models to follow will assume a protonated Glu83 and model the reaction mechanism found in Scheme 2b.

Reduction of HMG-CoA to Mevaldyl-CoA via a Hydride Transfer Mechanism. As discussed above, the theozyme and ONIOM approaches provide complementary views of the reaction mechanism. Figure 5 shows the reaction profiles for the hydride transfer reactions calculated with both methods. For the first hydride transfer reaction, the activation energy is calculated to be 26.8 kcal/mol for the theozyme model and 21.8 kcal/mol for the ONIOM model. We expect the theozyme models to overestimate this value relative to the ONIOM models because of the longer C_a−C_d distances in the reactant (4.4 Å) and product (4.2 Å). This may partially explain the 5 kcal/mol difference in activation energy calculated between the theozyme and ONIOM models. The reaction energies are calculated to be −0.8 and 8.3 kcal/mol by theozyme and ONIOM models, respectively. The difference in reaction energies likely represents upper and lower bounds of the actual value. The free energy obtained by the theozyme approach may be underestimated for the same reason described above, while the ONIOM value is overestimated because of a significant positive error observed in the MM/MM S-value test performed between the reactant and product states.[68] Figure 6 shows the structures of the reactant, transition state, and product from the theozyme calculations (a) and the ONIOM calculations (b). The position of the transferring hydrogen (H_t) between C_d and C_a in the transition state, with distances of 1.3 and 1.4 Å, respectively, is consistent with a thermoneutral reaction.

A comparison between the theozyme and ONIOM reactant structures in panels a and b of Figure 6, respectively, reveals the effects of the enzyme structure on the chemical reaction. The protein environment positions the thioester parallel to the NADH nicotinamide ring and equidistant (3.0 Å) from both

dx.doi.org/10.1021/bi3008593 | *Biochemistry* 2012, 51, 7983−7995

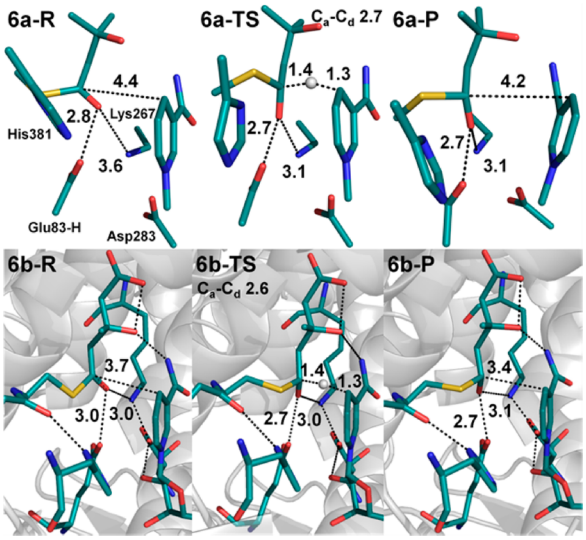

Figure 6. (a) Theozyme and (b) ONIOM models for the reactant, transition state, and product of the first hydride transfer when Glu83 is protonated.

residues in the oxyanion hole. Conversely, the thioester is not held parallel to the cofactor in the theozyme model, and the distance from the thioester to Lys267 increases from 3.0 to 3.6 Å. As a result, the theozyme structure does not produce an ideal Bürgi–Dunitz trajectory for the hydride transfer.[70] Therefore, part of the catalytic effect of the protein environment in addition to the stabilization of the developing negative charge is the proper positioning of the reaction partners.

The ONIOM models reveal why the hydrogen bond formed between the positively charged His381 and the carbonyl oxygen of the first peptide bond of HMG-CoA is important. This interaction rotates His381 away from the sulfur (3.0 Å from His δH), and the thioester adopts an orientation that is more suitable for hydride transfer. Because this interaction is absent in the theozyme models, His381 crowds the hemithioacetal sulfur through a weak electrostatic interaction (2.6 Å from His δH). The result of this crowding interaction is a rotation of the forming oxyanion toward Glu83, which enforces distorted hydrogen bonding angles between the oxyanion and Glu83 (125°) and Lys267 (138°). This rotation also forces H_t above the C_a–C_d line to maintain an ideal Bürgi–Dunitz type trajectory for attack of the hydride.[70] These structural differences could also rationalize the calculated energy differences between models.

It should be noted that the hydrogen bond between the first peptide bond of HMG-CoA and His381 is not observed in the available crystal structures. This is an interesting example of the synergy between X-ray crystallography and computational methods because the crystal structures do not describe the Michaelis complex. However, in conjunction, the computational models and crystal structures suggest a mechanism by which His381 and Ser85 can control the conformation of the first peptide bond, as shown in Scheme 3, that may be important for positioning substrates, intermediates, or products, even though it is not explicitly observed on the time scales probed by the MD simulations described here.[21] Nevertheless, the interaction between His381 and the first peptide bond itself is intriguing because it provides a direct contact between the reaction substrate and the flap domain. It also positions the catalytically important His381 close to the sulfur atom to

Scheme 3. Suggested Mechanism from MD Simulations and X-ray Crystallography for Control over the Conformation of the First Peptide Bond by residues Ser85 and His381[a]

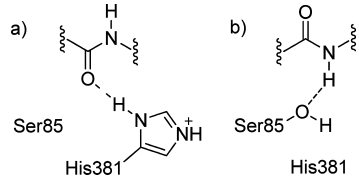

[a](a) Conformation observed in MD simulations of the Michaelis complex, where His381 hydrogen bonds to the carbonyl of the first peptide bond and the hydroxyl group of Ser85 is rotated away. (b) Conformation observed in the hemidithioacetal crystal structure, where the first peptide bond is rotated 180° and the amide nitrogen is hydrogen bonded to Ser85 while His381 is rotated away or deprotonated to remove its hydrogen bond donor.

conduct its function later in the reaction sequence. The distance between His381 and the sulfur atom of the substrate decreases from 4.1 to 3.5 Å after the hydride is transferred, suggesting it could play a small role in transition state stabilization through an electrostatic interaction. It is reasonable to expect that the negative charge of the oxyanion is delocalized onto the sulfur in the transition state. This finding also hints at a possible mechanism for the proton transfer process after breakdown of the hemithioacetal. As the C_a–S bond length increases and negative charge further accumulates on the sulfur, the hydrogen bond will become bifurcated until the bond is broken and the proton can be transferred to the CoA thiolate anion.

As expected, Glu83 and Lys267 form an oxyanion hole with distances of 2.7 and 3.0 Å, respectively, at the transition state to stabilize the developing negative charge on the thioester oxygen. In the product complex, Glu83 fully transfers its hydrogen to form a protonated, tetrahedral hemithioacetal intermediate. The imaginary frequency in the transition state for the hydride transfer corresponds to coupled movement between the transferring motion of the hydride from C_d to C_a and motions of the proton on Glu83 toward the forming oxyanion. The general acid in this reaction is most likely Glu83 as opposed to Lys267 based on the optimized product state, a shorter hydrogen bond, the coupled motion in the transition state vibrational mode, and the results from the theozyme models with deprotonated Glu83. Lys267 is important for transition state stabilization, and the salt bridge formed between it and Asp283 positions its essential positive charge in the oxyanion hole. In addition, Asp283 also forms a hydrogen bond with the 2′-hydroxy group of the ribose ring of the NAD cofactor, which in tandem with the hydrogen bond between the cofactor carboxyamide group and the 3-hydroxy group of HMG is likely to stabilize the position of the cofactor. These structural models have further refined the roles of the catalytic residues, and through the hydrogen bonding network described, they are consistent with the available experimental data.[11,12]

Additionally, the ONIOM structures suggest that the pK_a of Glu83 is at least partially modulated by the redox state of the cofactor. In the reactant, both species are neutral and separated by 3.3 Å, while in the product, they possess opposite charges and form a favorable 3.1 Å electrostatic interaction. These results are consistent with the previously suggested hypothesis that the redox state of the NAD cofactor is used by the enzyme to modulate the pK_a of important active site residues.[26,28] This

dx.doi.org/10.1021/bi3008593 | *Biochemistry* 2012, 51, 7983–7995

type of effect has, for example, been shown to influence the cofactor binding process of LADH.[71,72] The theozyme models are unable to reproduce these effects, demonstrating the control that the protein environment imposes on the chemical reaction.

Reduction of Mevaldehyde to Mevalonate via a Hydride Transfer Mechanism. The reaction energy profiles for the second hydride transfer reaction calculated with each method are shown on the right side of Figure 5. In these models, Glu83 is reprotonated after hemithioacetal breakdown and cofactor exchange due to the effect of NADH and Asp283 on the pK_a value of Glu83. It is also assumed that the CoA thiolate is protonated and maintains a hydrogen bond to His381 through the second hydride transfer reaction in accordance with the proper positioning described in the models above and the role of the residue proposed in the literature.[11,32] This hypothesis is supported by the fact that the interaction is maintained in MD simulations of the mevaldehyde−NADH complex and the experimental observation that the reduction of mevaldehyde to mevalonate is faster in the presence of CoA.[22] As might be expected from the higher electrophilicity of the aldehyde relative to that of the thioester in the first hydride transfer step, the barriers calculated for the reduction of mevaldehyde are lower than that of the reduction of the thioester of HMG-CoA. The theozyme and ONIOM models are in good agreement about the activation energy for the second reduction step, 19.3 and 19.1 kcal/mol, respectively. Again, the theozyme models likely overestimate the activation energy, with longer C_a−C_d distances in the reactant (4.2 Å) and product (3.9 Å) structures. However, the effect is not as pronounced as in the models for the first hydride transfer step. The calculated reaction energies for the theozyme and ONIOM models are 1.7 and −1.7 kcal/mol, respectively, differing by approximately 3 kcal/mol. It should be noted that the ONIOM calculations have a significant negative error in the MM/MM S-value test performed between the reactant and product states, making the calculated energies less reliable.[68] Figure 7 shows the reactant, transition state, and product structures from the theozyme calculations (a) and the ONIOM calculations (b) for the second hydride transfer reaction. The position of the H_t between C_d and C_a in the transition state, with distances of 1.4 and 1.3 Å, respectively, is consistent with a thermoneutral or slightly endothermic reaction.

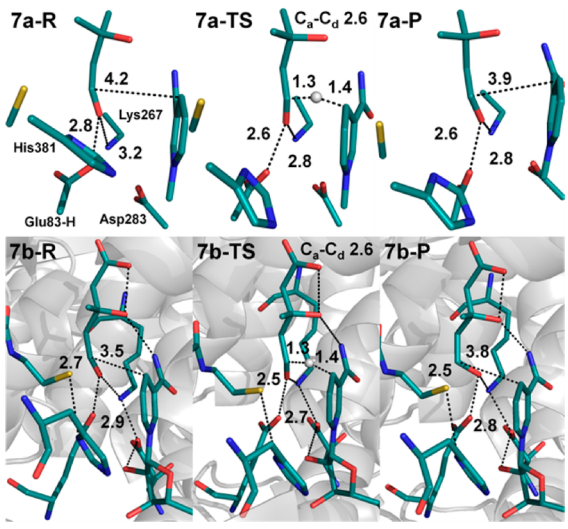

Figure 7. (a) Theozyme and (b) ONIOM models for the reactant, transition state, and product of the second hydride transfer reaction.

The geometry of the transition state for the second hydride transfer reaction is similar to that of the first hydride transfer reaction. It is interesting to note that the enzyme positions the CoA thiol group through interactions with Ser85 and His381 in the vicinity of the reactive center perhaps to maintain the general shape of the active site observed in the first hydride transfer. This could prevent the enzyme from needing to make significant changes to accommodate hydride transfer to a smaller, more mobile substrate. This rationalizes why a single active site can catalyze the hydride transfer to two sterically and electronically different substrates and why the presence of CoASH accelerates the reduction of mevaldehyde.[22,26,27] The oxyanion hole consisting of Glu83 and Lys267 binds to the transition state tighter than in the first hydride transfer reaction, forming 2.5 and 2.7 Å hydrogen bonds. This observation is consistent with the lower barrier to the reaction and the lack of delocalization of the negative charge, leading to a full negative charge on the oxygen atom in the transition state. Peripheral stabilization of the transition state is no longer needed, so deprotonation of His381 adjusts the electrostatic environment of the active site to accommodate the aldehyde substrate. In the product structures, Glu83 instantaneously donates a proton in the final protonation step of mevalonate. There is also significant coupling between the motions of the hydride and proton from Glu83 in the imaginary frequency of the transition state in both models. Corroborating the pK_a modulation hypothesis developed from the models of the first hydride transfer reaction, the distance between the cofactor and Glu83 is shorter in the ONIOM product structure (2.9 Å) than the reactant structure (3.2 Å). The ONIOM and theozyme models both predict a geometry in which mevalonate adopts a conformation in which the transferred hydrogen is rotated away from the cofactor. From this position, the enzyme would have to rotate mevalonate to perform the reverse reaction (oxidation of mevalonate). This mevalonate conformation is also observed and stable in the mevalonate−NAD^+ MD simulations.

Relative Stability of Structures along the Reaction Pathway. An open question about the mechanism of HMGR is the problem that mevaldehyde is postulated as a reaction intermediate and substrate for the second hydride transfer but was not detected in a series of experiments.[22−24] We therefore hypothesized that the active site stabilizes the hemithioacetal intermediate. To investigate this hypothesis, MD simulations were performed on the relevant enzyme−substrate−cofactor complexes along the reaction coordinate and 700−800 snapshots from the trajectories were examined using MM/PBSA rescoring. MM/PBSA is an efficient free energy calculation used to include contributions from solvation to the binding energy of a given set of ligands.[73,74] It is being used here to gain insight into the way the intermediates interact with the enzyme active site and gain a qualitative understanding of the relationship between the proposed complexes on the reaction coordinate. Figure 8 shows the relative binding energies of the combined substrate and cofactor determined from MM/PBSA rescoring along with the values from the van der Waals terms of the scoring function. These energy values are consistent with the energy values calculated for isolated substrates and cofactors as shown in Figure S3 of the Supporting Information.

dx.doi.org/10.1021/bi3008593 | *Biochemistry* 2012, 51, 7983−7995

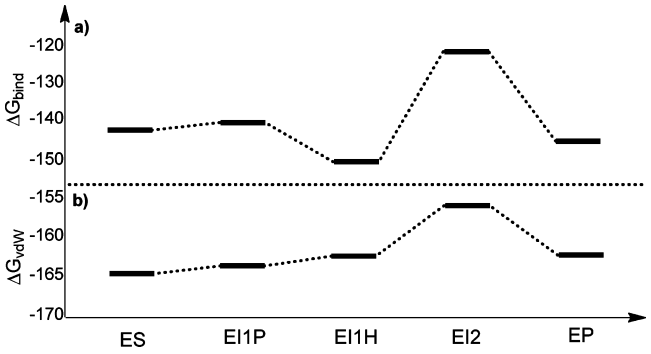

Figure 8. (a) Binding energies, ΔG_{bind}, and (b) van der Waals energies, ΔG_{vdW}, from MM/PBSA rescoring of the MD simulations performed for several structures along the model reaction coordinate.

The most striking result from these calculations is the prediction that the interaction in the mevaldehyde−NADH complex is less favorable than in the other complexes along the model reaction pathway. Of particular interest, both of the hemithioacetal complexes examined are lower in energy than the aldehyde complex. Although the ΔG_{bind} values in Figure 8a are dominated by the ΔG_{elec} and ΔG_{PB} terms, which may be hard to compare for species with different charge states, the ΔG_{vdW} values in Figure 8b also follow the same trends as the ΔG_{bind} values and are independent of the charge state of the complexes. This indicates that the hemithioacetal fits better into the active site than the aldehyde and provides an explanation for why the aldehyde is not observed experimentally. Also of interest is a comparison between the enzyme complexes with the hemithioacetal and different redox states of the enzyme. The rescoring results predict that the hemithioacetal−NADH complex is more favorable than the hemithioacetal−NAD^+ complex. This finding indicates the enzyme may thermodynamically favor cofactor exchange over the hemithioacetal breakdown reaction, although these methods do not consider the kinetics of the flap opening and closing process. These calculations are qualitatively consistent with experiment and provide a rationalization for the failure to observe the putative aldehyde intermediate as well as a starting point for further investigation into the reaction mechanism of HMGR between the hydride transfer mechanisms.

DISCUSSION

Revised Mechanism. The goal of these studies is to refine and expand what is known experimentally about the mechanism of HMG-CoA reductase and define the role of the individual active site residues to an atomistic level using computational methods. The models presented here indicate that Glu83 is protonated prior to hydride transfer, which is modulated by the negative charge of Asp283 and the redox state-dependent charge of the NAD cofactor. On the basis of this model, the catalytic roles of the conserved active site residues can then be refined as illustrated in Scheme 4. Glu83 acts as a part of the oxyanion hole and general acid in the final protonation step of mevalonate. Lys267 acts as the other part of the oxyanion hole and maintains its formal positive charge. The positions of these residues provide the enzyme with an oxyanion hole that can bind tightly to the developing negative charge in the transition states of both reactions. His381 forms a hydrogen bond with the carbonyl of the first peptide bond of HMG-CoA to position it to provide some transition state

Scheme 4. Revised Mechanism for *Pm*HMGR

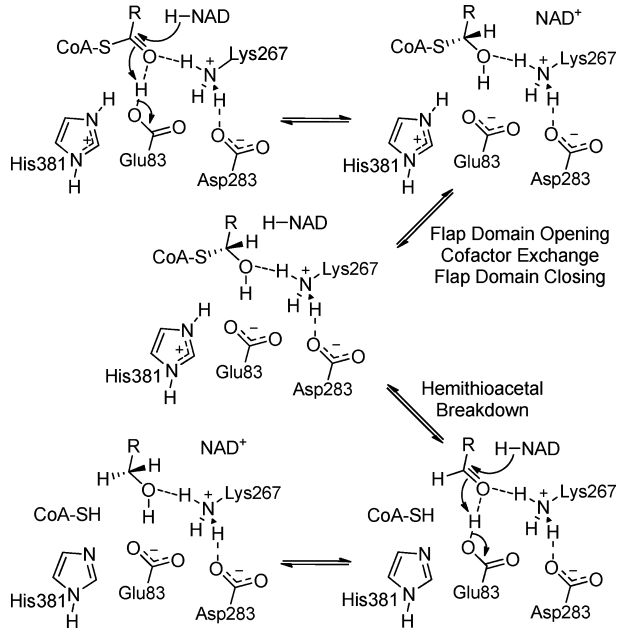

stabilization for the first hydride transfer and eventually protonate the CoA thiolate anion. It remains in contact with the CoASH, which is held in a position that sequesters the mobility of the aldehyde until the second hydride transfer can occur. Asp283 stabilizes the position of Lys267 in the oxyanion hole as well as the position of the cofactor through a hydrogen bond with the nicotinamide ribose ring.

The computational studies also provide some insight into the breakdown of the initial hemithioacetal intermediate. Results from kinetic experiments and the absence of the free aldehyde are consistent with the hypothesis that the cofactor exchange step occurs before breakdown of the hemithioacetal.[23−26] MM/PBSA free energy calculations indicate that the enzyme active site stabilizes the hemithioacetal relative to the aldehyde. Consequently, the opening−closing process of the flap domain and cofactor exchange must be faster than hemithioacetal breakdown after the thioester is reduced. By destabilizing the aldehyde, the enzyme is able to slow the hemithioacetal breakdown reaction, which is rapid in solution with CoA thiols,[75] to a point where the cofactor exchange is faster. The redox state of the cofactor could also play a role in limiting hemithioacetal breakdown. In the models employed, hemithioacetal breakdown necessarily involves reprotonation of Glu83, which could be obstructed by the favorable interaction between deprotonated Glu83 and the oxidized cofactor until the interaction is outcompeted by cofactor exchange. Slowing this process could be critical to the enzyme efficiency because mevaldehyde has been shown to be significantly hydrated (39%) in solution.[28] Thus, once the cofactor exchange step has been completed, the reaction can proceed without the aldehyde ever being exposed to solvent, thereby protecting it from hydration or other side reactions.[27]

The ONIOM activation energies for the two separate hydride transfer reactions, 21.8 and 19.1 kcal/mol, respectively, are in reasonable agreement with the experimentally determined time scale for the reaction, which is on the order of 1 s^{-1} to 1 m^{-1}.[22] This is consistent with the hypothesis that the first hydride transfer is the rate-limiting step of the enzyme, even though very little is known about the rates of the opening

dx.doi.org/10.1021/bi3008593 | *Biochemistry* 2012, 51, 7983−7995

and closing of the flap domain. It has been suggested from kinetic studies of the yeast HMGR that cofactor release after the second hydride transfer reaction is rate-limiting, which could be associated with large-scale domain movement.[26] Further experiments or modeling studies are required to estimate a rate constant for the flap movement. Assuming that the flap opening and closing process occurs on a time scale similar to or longer than that of the first hydride transfer, the second hydride transfer is the fastest of the three processes, rationalizing the observation that the aldehyde intermediate may not accumulate in any significant quantity.

Comparisons to the Hydride Transfer Reactions Catalyzed by LADH. One of the unique aspects of HMGR is the fact that two hydride transfers to two sterically and electronically different substrates occur in the same active site. It is therefore of interest to compare the mechanisms of the two individual steps to enzymes that catalyze only a single hydride transfer such as the well-studied NADH-dependent system of liver alcohol dehydrogenase. The redox activity of LADH occurs with a zinc cofactor and a proton relay system through highly conserved serine and histidine residues. This is in contrast with HMGR, which utilizes hydrogen bonding from active site residues, Glu83 and Lys267, for oxyanion stabilization and a single residue, Glu83, as the acid and base. Aldehyde oxidation catalyzed by LADH is comparable to the reaction catalyzed by aldehyde dehydrogenases, which have not yet been investigated computationally.[41] In these enzymes, a catalytic cysteine residue undergoes nucleophilic attack on the aldehyde substrate to form a covalent enzyme−substrate hemithioacetal. This species is then oxidized through hydride transfer to NAD^+ followed by hydrolysis of the thioester to give the acid product. LADH is thought to proceed on a similar reaction path with a zinc-bound hydroxide ion playing the role of cysteine.[41] Attack of this hydroxide ion on the aldehyde substrate produces an aldehyde hydrate that is oxidized by NAD^+. Alcohol oxidation by LADH similarly occurs from a zinc-bound substrate with the versatile proton relay system present to perform the necessary acid−base chemistry. The ancillary reaction mechanisms of LADH are quite different from that of HMGR, but the transition structure models are comparable because of the similarity of the chemical process involved. The reactions catalyzed by LADH are illustrated in Scheme 5.

The aldehyde oxidation reaction is compared to the first hydride transfer of HMGR. They involve hydride transfer with a zinc-coordinated aldehyde hydrate and hemithioacetal, respectively. Olsen et al. examined the hydride transfer reaction using short MD simulations and small theozyme models using the semiempirical PM3 method.[41] The MD simulations revealed an average distance of 2.56 Å between the acceptor carbon and the transferring hydrogen (C_a−H_t) of NAD over 100 ps. This compares with the C_a−C_d distances observed in our MD simulations (3.5 Å) for the first hydride transfer of HMGR. The calculated activation energy of 21.5 kcal/mol places this reaction in qualitative agreement with the ONIOM reaction barrier of 21.8 kcal/mol for HMGR, despite significant differences in the methods used.

A few extensive computational studies are of note for the alcohol oxidation step catalyzed by LADH.[39,40,42] Agarwal et al. performed MD simulations and theozyme models on the reduction of benzaldehyde by LADH using various methods. MD simulations of the reactant complex revealed an average C_a−C_d distance of 3.56 Å over 100 ps. This compares with the

Scheme 5. Reactions Catalyzed by Liver Alcohol Dehydrogenase[a]

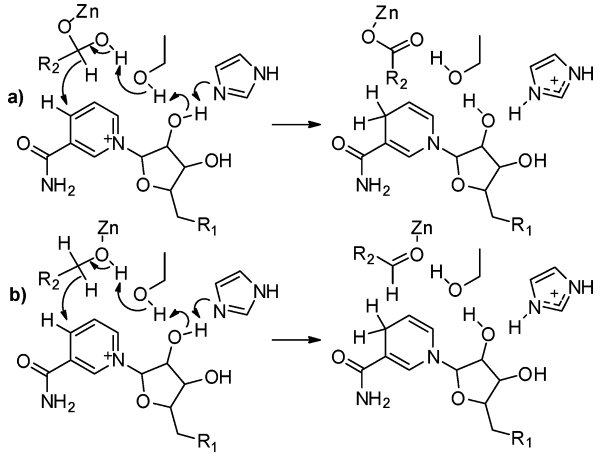

[a](a) Oxidation of aldehyde hydrate to zinc-bound acid and (b) oxidation of alcohol to aldehyde.

average C_a−C_d distance (3.3 Å) in our MD simulations for the second hydride transfer reaction of HMGR. The hydride transfer transition structures are compared in Figure 9. While

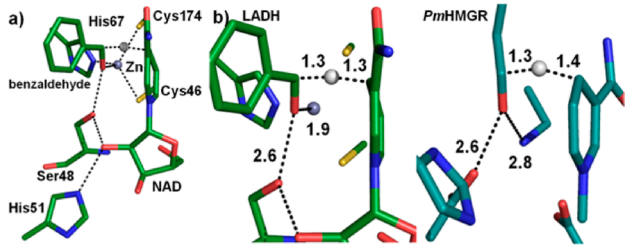

Figure 9. (a) Theozyme model of the transition state of hydride transfer to benzaldehyde by LADH.[39] (b) Comparison of the LADH transition state (left) to the theozyme model hydride transfer to mevaldehyde catalyzed by *Pm*HMGR (right; see Figure 7a) with important distances shown. Hydrogen atoms were omitted for the sake of clarity.

the reaction mechanisms are very different, the three-dimensional transition structure models are similar. The acid−base chemistry performed by Glu83 in HMGR is analogous to the function of the proton relay consisting of Ser48, the cofactor ribose hydroxyl group, and His51 in LADH. The proton relay system and Glu83 also provide a similar degree of transition state stabilization through hydrogen bonding with bond distances of approximately 2.6 Å. The essential positive charge provided by Lys267 and supported by Asp283 for *Pm*HMGR is provided by the zinc cofactor in LADH and supported by coordinating cysteine and histidine residues. Despite the vast differences in the identities of the groups assembled around the transition state for stabilization, H_t is positioned similarly between C_a and C_d for both reactions. Some of the major differences between these reactions are stereochemical. The hydride is transferred to opposite faces of the aldehyde and from opposite faces of the cofactor. These differences are geometrically dictated by the construction of the enzyme active site and likely have only slight effects on the transition states themselves.

The LADH barrier height was calculated to be 21.9 kcal/mol at the B3LYP/6-31G**//RHF/3-21G level of theory, which is

dx.doi.org/10.1021/bi3008593 | *Biochemistry* 2012, 51, 7983−7995

also in qualitative agreement with the results for HMGR.[39] However, Cui et al. performed QM/MM calculations on ethanol oxidation by LADH using the DFT-based semi-empirical self-consistent charge-density-functional-tight-binding (SCC-DFTB) method and the CHARMM force field.[40] They obtained a much lower barrier of 9.4 kcal/mol and attributed the difference from the results of Agarwal et al. to inclusion of the protein environment and the sensitivity of the effect of the C_a-C_d distance on barrier height. Some difference may also be attributed to the different substrates that were used. Regardless, this value is approximately 10 kcal/mol lower than the ONIOM value calculated for the second hydride transfer of HMGR, which might be at least partially a consequence of the tight-binding approach using the SCC-DFTB method. It must be noted that the importance of quantum tunneling effects on the catalysis of LADH is significant and any tunneling effects for the hydride transfer reactions of HMGR are ignored in these studies.[40,42] Thus, the barriers calculated here may represent upper bounds in comparing our energy values to any experimentally determined kinetic parameters.

CONCLUSIONS

Reported here is a computational investigation into the hydride transfer mechanisms for the double reduction of HMG-CoA catalyzed by *Pm*HMGR. It is shown that the charge state of the catalytic residue Glu83 is most likely neutral before either hydride transfer. Glu83 also functions as the acid group to protonate the reduced thioester and aldehyde, while Lys267 donates another hydrogen bond to the oxyanion hole for transition state stabilization. Small rearrangements of the active site are observed in the models that allow the enzyme to catalyze hydride transfer to two different substrates in sequence. The QM/MM calculations predict reaction barriers for the hydride transfer steps of 21.8 and 19.1 kcal/mol, respectively, which agree with the experimentally observed rate. Some insight into the flap opening and cofactor exchange events between the hydride transfer reactions has been gained. Consistent with experiment, MM/PBSA rescoring predicts that the active site is more suited for binding the hemithioacetal intermediate, which may be to protect the aldehyde intermediate from solvent. Thus, the enzyme must slow the hemithioacetal−aldehyde conversion. Potential mechanisms have been identified as destabilization of the aldehyde and fine-tuning of the protonation state of Glu83. After cofactor exchange and after the solvent has been excluded from the active site, His381 is in position through hydrogen bonding with the substrate to protonate the CoA thiolate anion.

HMGR catalyzes a complex hydride transfer sequence through a mechanism different from that of the hydride transfer enzymes studied in the literature. However, our calculations on the reduction steps of *Pm*HMGR are directly comparable to the computational studies performed on the mechanism of LADH. The calculations of the thioester reduction step are potentially applicable to other important redox active enzymes that proceed through intermediates of a similar type. Some of them include other oxidoreductases, such as cinnamoyl-CoA reductase,[76] aldehyde dehydrogenases and other members of the short chain dehydrogenase/reductase (SDR) superfamily,[77,78] fatty acyl-CoA reductases[79,80] and nitrile reductases,[81,82] which proceed through a four-electron reduction process similar to that of HMGR, and the reductase domains of polyketide synthases (PKS) and nonribosomal peptide synthetases (NRPS) that govern the release of complex natural products from the assembly machinery.[83−85]

ASSOCIATED CONTENT

Supporting Information

Additional references, additional figures, including an example theozyme model and root-mean-square deviation and distance plots from MD simulations, additional tables, and coordinates for theozyme models and atoms in the QM region of the ONIOM models. This material is available free of charge via the Internet at http://pubs.acs.org.

AUTHOR INFORMATION

Corresponding Author

*E-mail: owiest@nd.edu. Phone: (574) 631-5876.

Funding

This research was supported by a Graduate Fellowship from the Chemistry-Biochemistry-Biology Interface Program at the University of Notre Dame (National Institute of General Medical Sciences Grant T32-075762) to B.E.H.

Notes

The authors declare no competing financial interest.

ACKNOWLEDGMENTS

We thank the Center for Research Computing (CRC) at the University of Notre Dame and the National Science Foundation (TG-CHE090124) for generous allocation of computational resources. The computations used the Extreme Science and Engineering Discovery Environment (XSEDE), which is supported by National Science Foundation Grant OCI-1053575, and were performed on Kraken at the National Institute for Computational Sciences (http://www.nics.tennessee.edu/).

REFERENCES

(1) Miziorko, H. M. (2011) Enzymes of the mevalonate pathway of isoprenoid biosynthesis. *Arch. Biochem. Biophys. 505*, 131−143.

(2) Liao, J. K., Wang, C. Y., and Liu, P. Y. (2008) Pleiotropic effects of statin therapy: Molecular mechanisms and clinical results. *Trends Mol. Med. 14*, 37−44.

(3) Feng, L. L., Zhou, L., Sun, Y., Gui, J., Wang, X. F., Wu, P., Wan, J., Ren, Y. L., Qiu, S. X., Wei, X. Y., and Li, J. (2011) Specific inhibitions of annonaceous acetogenins on class II 3-hydroxy-3-methylglutaryl coenzyme A reductase from *Streptococcus pneumoniae*. *Bioorg. Med. Chem. 19*, 3512−3519.

(4) Hedl, M., and Rodwell, V. W. (2004) Inhibition of the Class II HMG-CoA reductase of *Pseudomonas mevalonii*. *Protein Sci. 13*, 1693−1697.

(5) Li, D., Gui, J., Li, Y., Feng, L., Han, X., Sun, Y., Sun, T., Chen, Z., Cao, Y., Zhang, Y., Zhou, L., Hu, X., Ren, Y., and Wan, J. (2012) Structure-Based Design and Screen of Novel Inhibitors for Class II 3-Hydroxy-3-methylglutaryl Coenzyme A Reductase from *Streptococcus pneumoniae*. *J. Chem. Inf. Model. 52*, 1833−1841.

(6) Medina-Franco, J. L., Singh, N., Tamariz, J., and Chamorro, G. (2009) Inhibitors of HMG-CoA Reductase: Current and Future Prospects. *Mini-Rev. Med. Chem. 9*, 1272−1283.

(7) Tobert, J. A. (2003) Lovastatin and beyond: The history of the HMG-CoA reductase inhibitors. *Nat. Rev. Drug Discovery 2*, 517−526.

(8) Burg, J. S., and Espenshade, P. J. (2011) Regulation of HMG-CoA reductase in mammals and yeast. *Prog. Lipid Res. 50*, 403−410.

(9) Istvan, E. S., Palnitkar, M., Buchanan, S. K., and Deisenhofer, J. (2000) Crystal structure of the catalytic portion of human HMG-CoA reductase: Insights into regulation of activity and catalysis. *EMBO J. 19*, 819−830.

(10) Istvan, E. S., and Deisenhofer, J. (2000) The structure of the catalytic portion of human HMG-CoA reductase. *Biochim. Biophys. Acta 1529*, 9−18.
(11) Tabernero, L., Bochar, D. A., Rodwell, V. W., and Stauffacher, C. V. (1999) Substrate-induced closure of the flap domain in the ternary complex structures provides insights into the mechanism of catalysis by 3-hydroxy-3-methylglutaryl-CoA reductase. *Proc. Natl. Acad. Sci. U.S.A. 96*, 7167−7171.
(12) Lawrence, C. M., Rodwell, V. W., and Stauffacher, C. V. (1995) Crystal-Structure of *Pseudomonas mevalonii* HMG-CoA Reductase at 3.0 Å Resolution. *Science 268*, 1758−1762.
(13) Fimognari, G. M., and Rodwell, V. W. (1965) Substrate-Competetive Inhibition of Bacterial Mevalonate:Nicotinamide-Adenine Dinucleotide Oxidoreductase (acylating CoA). *Biochemistry 4*, 2086−2090.
(14) Istvan, E. S. (2001) Bacterial and mammalian HMG-CoA reductases: Related enzymes with distinct architectures. *Curr. Opin. Struct. Biol. 11*, 746−751.
(15) Bochar, D. A., Stauffacher, C. V., and Rodwell, V. W. (1999) Sequence comparisons reveal two classes of 3-hydroxy-3-methylglutaryl coenzyme A reductase. *Mol. Genet. Metab. 66*, 122−127.
(16) Friesen, J. A., Lawrence, C. M., Stauffacher, C. V., and Rodwell, V. W. (1996) Structural determinants of nucleotide coenzyme specificity in the distinctive dinucleotide binding fold of HMG-CoA reductase from *Pseudomonas mevalonii*. *Biochemistry 35*, 11945−11950.
(17) Dugan, R. E., and Porter, J. W. (1971) Stereospecificity of the transfer of hydrogen from reduced nicotinamide adenine dinucleotide phosphate in each of the two reductive steps catalyzed by *β*-hydroxy-*β*-methylglutaryl coenzyme A reductase. *J. Biol. Chem. 246*, 5361−5364.
(18) Beedle, A. S., Munday, K. A., and Wilton, D. C. (1972) The stereochemistry of hydrogen transfer from NADPH catalysed by 3-hydroxy-3-methylglutaryl-coenzyme A reductase from rat liver. *Eur. J. Biochem. 28*, 151−155.
(19) Retey, J., Stetten, E. V., Coy, U., and Lynen, F. (1970) A Probable Intermediate in Enzymic Reduction of 3-Hydroxy-3-Methylglutaryl Coenzyme-A. *Eur. J. Biochem. 15*, 72−76.
(20) Beedle, A. S., Munday, K. A., and Wilton, D. C. (1972) The stereochemistry of the reduction of mevaldic acid-coenzyme A hemithioacetal by rat liver 3-hydroxy-3-methylglutaryl coenzyme A reductase. *FEBS Lett. 28*, 13−15.
(21) Steussy, C. N. C., Schmidt, T., Wrensford, L. V., Burgner, J. B., II, Rodwell, V. W., and Stauffacher, C. V. Coenzyme A as Catalyst. *J. Biol. Chem.*, submitted for publication.
(22) Jordanstarck, T. C., and Rodwell, V. W. (1989) *Pseudomonas mevalonii* 3-Hydroxy-3-Methylglutaryl-CoA Reductase: Characterization and Chemical Modification. *J. Biol. Chem. 264*, 17913−17918.
(23) Durr, I. F., and Rudney, H. (1960) Reduction of *β*-Hydroxy-*β*-methylglutaryl Coenzyme-A to Mevalonic Acid. *J. Biol. Chem. 235*, 2572−2578.
(24) Knappe, J., Ringelmann, E., and Lynen, F. (1959) Uber Die *β*-Hydroxy-*β*-Methyl-Glutaryl-Reduktase Der Hefe: Zur Biosynthese Der Terpene. 9. *Biochem. Z. 332*, 195−213.
(25) Bensch, W. R., and Rodwell, V. W. (1970) Purification and Properties of 3-Hydroxy-3-Methylglutaryl Coenzyme-A Reductase from *Pseudomonas*. *J. Biol. Chem. 245*, 3755−3762.
(26) Qureshi, N., Dugan, R. E., Cleland, W. W., and Porter, J. W. (1976) Kinetic analysis of the individual reductive steps catalyzed by *β*-hydroxy-*β*-methylglutaryl-coenzyme A reductase obtained from yeast. *Biochemistry 15*, 4191−4107.
(27) Duncan, C. (2009) Analysis of the HMG-CoA reductase reaction mechanism by X-ray crystallography. Ph.D. Thesis, Purdue University, West Lafayette, IN.
(28) Veloso, D., Cleland, W. W., and Porter, J. W. (1981) pH Properties and Chemical Mechanism of Action of 3-Hydroxy-3-methylglutaryl Coenzyme-A Reductase. *Biochemistry 20*, 887−894.
(29) Wang, Y. L., Darnay, B. G., and Rodwell, V. W. (1990) Identification of the Principal Catalytically Important Acidic Residue of 3-Hydroxy-3-methylglutaryl Coenzyme-A Reductase. *J. Biol. Chem. 265*, 21634−21641.
(30) Darnay, B. G., Wang, Y. L., and Rodwell, V. W. (1992) Identification of the Catalytically Important Histidine of 3-Hydroxy-3-methylglutaryl-Coenzyme-A Reductase. *J. Biol. Chem. 267*, 15064−15070.
(31) Darnay, B. G., and Rodwell, V. W. (1993) His(865) Is the Catalytically Important Histidyl Residue of Syrian-Hamster 3-Hydroxy-3-methylglutaryl-Coenzyme-A Reductase. *J. Biol. Chem. 268*, 8429−8435.
(32) Frimpong, K., and Rodwell, V. W. (1994) Catalysis by Syrian-Hamster 3-Hydroxy-3-methylglutaryl-Coenzyme-A Reductase: Proposed Roles of Histidine-865, Glutamate-558, and Aspartate-766. *J. Biol. Chem. 269*, 11478−11483.
(33) Lawrence, C. M., Chi, Y. I., Rodwell, V. W., and Stauffacher, C. V. (1995) Crystallization of HMG-CoA Reductase from *Pseudomonas mevalonii*. *Acta Crystallogr. D51*, 386−389.
(34) Bochar, D. A., Tabernero, L., Stauffacher, C. V., and Rodwell, V. W. (1999) Aminoethylcysteine can replace the function of the essential active site lysine of *Pseudomonas mevalonii* 3-hydroxy-3-methylglutaryl coenzyme A reductase. *Biochemistry 38*, 8879−8883.
(35) Nagel, Z. D., and Klinman, J. P. (2006) Tunneling and dynamics in enzymatic hydride transfer. *Chem. Rev. 106*, 3095−3118.
(36) Hammes, G. G., Benkovic, S. J., and Hammes-Schiffer, S. (2011) Flexibility, Diversity, and Cooperativity: Pillars of Enzyme Catalysis. *Biochemistry 50*, 10422−10430.
(37) McGeagh, J. D., Ranaghan, K. E., and Mulholland, A. J. (2011) Protein dynamics and enzyme catalysis: Insights from simulations. *Biochim. Biophys. Acta 1814*, 1077−1092.
(38) Hay, S., and Scrutton, N. S. (2012) Good vibrations in enzyme-catalysed reactions. *Nat. Chem. 4*, 161−168.
(39) Agarwal, P. K., Webb, S. P., and Hammes-Schiffer, S. (2000) Computational studies of the mechanism for proton and hydride transfer in liver alcohol dehydrogenase. *J. Am. Chem. Soc. 122*, 4803−4812.
(40) Cui, Q., Elstner, M., and Karplus, M. (2002) A theoretical analysis of the proton and hydride transfer in liver alcohol dehydrogenase (LADH). *J. Phys. Chem. B 106*, 2721−2740.
(41) Olson, L. P., Luo, J., Almarsson, O., and Bruice, T. C. (1996) Mechanism of aldehyde oxidation catalyzed by horse liver alcohol dehydrogenase. *Biochemistry 35*, 9782−9791.
(42) Allhambra, C., Corchado, J. C., Sanchez, M. L., Gao, J. L., and Truhlar, D. G. (2000) Quantum dynamics of hydride transfer in enzyme catalysis. *J. Am. Chem. Soc. 122*, 8197−8203.
(43) Pavelites, J. J., Gao, J. L., Bash, P. A., and Mackerell, A. D. (1997) A molecular mechanics force field for NAD^+, NADH, and the pyrophosphate groups of nucleotides. *J. Comput. Chem. 18*, 221−239.
(44) Klug, D. R., Walker, R. C., de Souza, M. M., Mercer, I. P., and Gould, I. R. (2002) Large and fast relaxations inside a protein: Calculation and measurement of reorganization energies in alcohol dehydrogenase. *J. Phys. Chem. B 106*, 11658−11665.
(45) Please see section 1 of the Supporting Information.
(46) Bayly, C. I., Cieplak, P., Cornell, W. D., and Kollman, P. A. (1993) A Well-Behaved Electrostatic Potential Based Method Using Charge Restraints for Deriving Atomic Charges: The RESP Model. *J. Phys. Chem. 97*, 10269−10280.
(47) Pearlman, D. A., Case, D. A., Caldwell, J. W., Ross, W. S., Cheatham, T. E., Debolt, S., Ferguson, D., Seibel, G., and Kollman, P. (1995) Amber, a Package of Computer-Programs for Applying Molecular Mechanics, Normal-Mode Analysis, Molecular-Dynamics and Free-Energy Calculations to Simulate the Structural and Energetic Properties of Molecules. *Comput. Phys. Commun. 91*, 1−41.
(48) Fox, T., and Kollman, P. A. (1998) Application of the RESP methodology in the parametrization of organic solvents. *J. Phys. Chem. B 102*, 8070−8079.
(49) Gordon, J. C., Myers, J. B., Folta, T., Shoja, V., Heath, L. S., and Onufriev, A. (2005) H++: A server for estimating pK_as and adding missing hydrogens to macromolecules. *Nucleic Acids Res. 33*, W368−W371.

(50) Myers, J., Grothaus, G., Narayanan, S., and Onufriev, A. (2006) A simple clustering algorithm can be accurate enough for use in calculations of pKs in macromolecules. *Proteins 63*, 928−938.
(51) Jorgensen, W. L., Chandrasekhar, J., Madura, J. D., Impey, R. W., and Klein, M. L. (1983) Comparison of Simple Potential Functions for Simulating Liquid Water. *J. Chem. Phys. 79*, 926−935.
(52) Duan, Y., Wu, C., Chowdhury, S., Lee, M. C., Xiong, G. M., Zhang, W., Yang, R., Cieplak, P., Luo, R., Lee, T., Caldwell, J., Wang, J. M., and Kollman, P. (2003) A point-charge force field for molecular mechanics simulations of proteins based on condensed-phase quantum mechanical calculations. *J. Comput. Chem. 24*, 1999−2012.
(53) Wang, J. M., Wolf, R. M., Caldwell, J. W., Kollman, P. A., and Case, D. A. (2004) Development and testing of a general Amber force field. *J. Comput. Chem. 25*, 1157−1174.
(54) Ryckaert, J. P., Ciccotti, G., and Berendsen, H. J. C. (1977) Numerical-Integration of Cartesian Equations of Motion of a System with Constraints: Molecular Dynamics of N-Alkanes. *J. Comput. Phys. 23*, 327−341.
(55) Vangunsteren, W. F., and Berendsen, H. J. C. (1977) Algorithms for Macromolecular Dynamics and Constraint Dynamics. *Mol. Phys. 34*, 1311−1327.
(56) Berendsen, H. J. C., Postma, J. P. M., Vangunsteren, W. F., Dinola, A., and Haak, J. R. (1984) Molecular-Dynamics with Coupling to an External Bath. *J. Chem. Phys. 81*, 3684−3690.
(57) Essmann, U., Perera, L., Berkowitz, M. L., Darden, T., Lee, H., and Pedersen, L. G. (1995) A Smooth Particle Mesh Ewald Method. *J. Chem. Phys. 103*, 8577−8593.
(58) Petersen, H. G. (1995) Accuracy and Efficiency of the Particle Mesh Ewald Method. *J. Chem. Phys. 103*, 3668−3679.
(59) Tantillo, D. J., Chen, J. G., and Houk, K. N. (1998) Theozymes and compuzymes: Theoretical models for biological catalysis. *Curr. Opin. Chem. Biol. 2*, 743−750.
(60) Dechancie, J., Clemente, F. R., Smith, A. J. T., Gunaydin, H., Zhao, Y. L., Zhang, X. Y., and Houk, N. (2007) How similar are enzyme active site geometries derived from quantum mechanical theozymes to crystal structures of enzyme-inhibitor complexes? Implications for enzyme design. *Protein Sci. 16*, 1851−1866.
(61) Hu, H., and Yang, W. T. (2008) Free energies of chemical reactions in solution and in enzymes with ab initio quantum mechanics/molecular mechanics methods. *Annu. Rev. Phys. Chem. 59*, 573−601.
(62) Cances, E., Mennucci, B., and Tomasi, J. (1997) A new integral equation formalism for the polarizable continuum model: Theoretical background and applications to isotropic and anisotropic dielectrics. *J. Chem. Phys. 107*, 3032−3041.
(63) Mennucci, B., and Tomasi, J. (1997) Continuum solvation models: A new approach to the problem of solute's charge distribution and cavity boundaries. *J. Chem. Phys. 106*, 5151−5158.
(64) Cossi, M., Barone, V., Mennucci, B., and Tomasi, J. (1998) Ab initio study of ionic solutions by a polarizable continuum dielectric model. *Chem. Phys. Lett. 286*, 253−260.
(65) Nakamura, H., Sakamoto, T., and Wada, A. (1988) A Theoretical Study of the Dielectric Constant of Protein. *Protein Eng. 2*, 177−183.
(66) Wiest, O., and Houk, K. N. (1995) Stabilization of the Transition-State of the Chorismate-Prephenate Rearrangement: An Ab-Initio Study of Enzyme and Antibody Catalysis. *J. Am. Chem. Soc. 117*, 11628−11639.
(67) Dapprich, S., Komaromi, I., Byun, K. S., Morokuma, K., and Frisch, M. J. (1999) A new ONIOM implementation in Gaussian98. Part I. The calculation of energies, gradients, vibrational frequencies and electric field derivatives. *THEOCHEM 461*, 1−21.
(68) Vreven, T., Byun, K. S., Komaromi, I., Dapprich, S., Montgomery, J. A., Morokuma, K., and Frisch, M. J. (2006) Combining quantum mechanics methods with molecular mechanics methods in ONIOM. *J. Chem. Theory Comput. 2*, 815−826.
(69) Tao, P., Fisher, J. F., Shi, Q. C., Vreven, T., Mobashery, S., and Schlegel, H. B. (2009) Matrix Metalloproteinase 2 Inhibition: Combined Quantum Mechanics and Molecular Mechanics Studies of the Inhibition Mechanism of (4-Phenoxyphenylsulfonyl)-methylthiirane and Its Oxirane Analogue. *Biochemistry 48*, 9839−9847.
(70) Burgi, H. B., Lehn, J. M., and Wipff, G. (1974) Chemical-Reaction Paths. 3. Ab-Initio Study of Nucleophilic Addition to a Carbonyl Group. *J. Am. Chem. Soc. 96*, 1956−1957.
(71) Coleman, P. L., Weiner, H., and Iweibo, I. (1972) Role of Zinc in Horse Liver Alcohol-Dehydrogenase: Influence on Structure and Conformational Changes. *Biochemistry 11*, 1010−1018.
(72) Andersson, P., Kvassman, J., Olden, B., and Pettersson, G. (1984) Electrostatic-Field Effects of Coenzymes on Ligand-Binding to Catalytic Zinc in Liver Alcohol-Dehydrogenase. *Eur. J. Biochem. 138*, 603−609.
(73) Kollman, P. A., Massova, I., Reyes, C., Kuhn, B., Huo, S. H., Chong, L., Lee, M., Lee, T., Duan, Y., Wang, W., Donini, O., Cieplak, P., Srinivasan, J., Case, D. A., and Cheatham, T. E. (2000) Calculating structures and free energies of complex molecules: Combining molecular mechanics and continuum models. *Acc. Chem. Res. 33*, 889−897.
(74) Wang, J. M., Hou, T. J., and Xu, X. J. (2006) Recent Advances in Free Energy Calculations with a Combination of Molecular Mechanics and Continuum Models. *Curr. Comput.-Aided Drug Des. 2*, 287−306.
(75) Schwartz, B., Vogel, K. W., and Drueckhammer, D. G. (1996) Coenzyme A hemithioacetals as easily prepared inhibitors of CoA ester-utilizing enzymes. *J. Org. Chem. 61*, 9356−9361.
(76) Sarni, F., Grand, C., and Boudet, A. M. (1984) Purification and Properties of Cinnamoyl-CoA Reductase and Cinnamyl Alcohol-Dehydrogenase from Poplar Stems (Populus-X-Euramericana). *Eur. J. Biochem. 139*, 259−265.
(77) Jornvall, H., Persson, B., Krook, M., Atrian, S., Gonzalezduarte, R., Jeffery, J., and Ghosh, D. (1995) Short-Chain Dehydrogenases Reductases (SDR). *Biochemistry 34*, 6003−6013.
(78) Bray, J. E., Marsden, B. D., and Oppermann, U. (2009) The human short-chain dehydrogenase/reductase (SDR) superfamily: A bioinformatics summary. *Chem.-Biol. Interact. 178*, 99−109.
(79) Hofvander, P., Doan, T. T. P., and Hamberg, M. (2011) A prokaryotic acyl-CoA reductase performing reduction of fatty acyl-CoA to fatty alcohol. *FEBS Lett. 585*, 3538−3543.
(80) Willis, R. M., Wahlen, B. D., Seefeldt, L. C., and Barney, B. M. (2011) Characterization of a Fatty Acyl-CoA Reductase from *Marinobacter aquaeolei* VT8: A Bacterial Enzyme Catalyzing the Reduction of Fatty Acyl-CoA to Fatty Alcohol. *Biochemistry 50*, 10550−10558.
(81) Chikwana, V. M., Stec, B., Lee, B. W., de Crecy-Lagard, V., Iwata-Reuyl, D., and Swairjo, M. A. (2012) Structural basis of biological nitrile reduction. *J. Biol. Chem. 287*, 30560−30570.
(82) Kim, Y., Zhou, M., Moy, S., Morales, J., Cunningham, M. A., and Joachimiak, A. (2010) High-resolution structure of the nitrile reductase QueF combined with molecular simulations provide insight into enzyme mechanism. *J. Mol. Biol. 404*, 127−137.
(83) Fischbach, M. A., and Walsh, C. T. (2006) Assembly-line enzymology for polyketide and nonribosomal peptide antibiotics: Logic, machinery, and mechanisms. *Chem. Rev. 106*, 3468−3496.
(84) Chhabra, A., Haque, A. S., Pal, R. K., Goyal, A., Rai, R., Joshi, S., Panjikar, S., Pasha, S., Sankaranarayanan, R., and Gokhale, R. S. (2012) Nonprocessive [2 + 2]e- off-loading reductase domains from mycobacterial nonribosomal peptide synthetases. *Proc. Natl. Acad. Sci. U.S.A. 109*, 5681−5686.
(85) Du, L., and Lou, L. (2010) PKS and NRPS release mechanisms. *Nat. Prod. Rep. 27*, 255−278.